Comparison of Separation Performance of a Structured Packed Column with a Tray-Type Column for H_2S and CO_2

M. Baniadam, J. Fathikalajahi* and M.R. Rahimpour

Chemical and Petroleum Engineering Department, Shiraz University, Shiraz – Iran
e-mail: baniadam@shirazu.ac.ir - fathi@shirazu.ac.ir - rahimpour@shirazu.ac.ir

* Corresponding author

Résumé — **Comparaison des performances de séparation d'une colonne à garnissage structurée avec celles d'une colonne à plateaux pour l'H_2S et le CO_2** — L'absorption de gaz acides, H_2S et CO_2, par la méthyldiéthanolamine dans une colonne à garnissage structure équipée du Montz-Pak A3-500 a été modélisée mathématiquement. Les dimensions des canaux ainsi que leur nombre et le modèle d'écoulement du film liquide sont similaires à ceux des travaux de Shilkin. Les équations de transfert de la chaleur et de la masse sont dérivées pour le film liquide de réaction et le gaz qui s'écoule à contre-courant dans la colonne. La répartition de la concentration est calculée sur tout le film liquide en mouvement et aucune zone présentant des conditions de concentration équilibrée n'est prise en compte dans le liquide réactif. Les résultats du modèle pour la colonne structurée montrent de meilleures performances d'absorption du H_2S qu'avec une colonne à plateaux dans les mêmes conditions. Les résultats obtenus par le modèle indiquent une répartition appréciable de la répartition de la concentration et de la température le long de la colonne.

Abstract — *Comparison of Separation Performance of a Structured Packed Column with a Tray-Type Column for H_2S and CO_2 – Absorption of acid gases, H_2S and CO_2, by methyl diethanol amine in a structured packed column equipped with Montz-Pak A3-500 was mathematically modeled. The dimensions of the channels as well as their number and liquid film flow model are similar to the Shilkin's work. Heat and mass transfer equations are derived for reacting liquid film and gas flowing counter-currently into the column. Concentration distribution is calculated across the moving liquid film and no zone with equilibrium concentration conditions is considered in the reacting liquid. The results of the model for the structured column show a better performance for H_2S absorption compared with a tray column operating in the same conditions. The results obtained by the model indicate appreciable distribution of concentration and temperature along the column.*

NOMENCLATURE

a_e effective mass transfer area to packing volume (m^2/m^3)

a_t interfacial area to packing volume (m^2/m^3)

A coefficient defined in Equation (4)

b width of corrugation normal to column axis (m)

b_0 width of corrugation normal to direction of flow (m)

B coefficient defined in Equation (4)

C coefficient defined in Equation (4)

C concentration ($mole/m^3$)

CA_1 concentration of CO_2 in liquid ($mole/m^3$)

CA_2 concentration of H_2S in liquid ($mole/m^3$)

CB_2 concentration of MDEA in liquid ($mole/m^3$)

CE_2 concentration of HCO_3^- in liquid ($mole/m^3$)

CE_3 concentration of HS^- in liquid ($mole/m^3$)

CF_2 concentration of $MDEAH^+$ in liquid ($mole/m^3$)

C_p specific heat (J/mol.K)

d_h hydraulic diameter of channels (m)

D diffusion coefficient (m^2/s)

$\bar{D}$ molar average diffusion coefficient (m^2/s)

D_{pac} packing diameter (m)

F mole flow rate (kmole/h)

g gravity acceleration (m/s^2)

h corrugation height (m)

h_i^{ex} excess molar enthalpy (J/mole)

h_i^{is} ideal solution molar enthalpy (J/mole)

$\bar{h}_i^{liq}$ partial molar enthalpy of component i in liquid (J/mole)

K reaction equilibrium constant

k_L mass transfer coefficient (m/s)

L mole flow rate of liquid (mole/s)

L height of packing segment (m)

$\dot{m}$ mass flow rate (kg/s)

$\bar{M}$ average molecular weight

P pressure (Pa)

q volume flow rate (m^3/s)

R gas constant (J/mole.K)

Rh hydraulic radius of channels (m)

s width of corrugation side normal to column axis (m)

s_0 width of corrugation side normal to direction of flow (m)

S_e packing effective (wetted) mass transfer area (m^2)

S_t packing geometric (installed) area (m^2)

T temperature (K)

u velocity (m/s)

$\mathbf{v}$ velocity vector (m/s)

V mole flow rate of gas (mole/s)

w_G width of total area in a packing cross-section (m)

w_L width of wetted area in a packing cross-section (m)

x Cartesian coordinate, mole fraction of liquid

y Cartesian coordinate, mole fraction of gas

z mixing length (m)

Greek letters

α gravity flow angle (°)

γ angle between column axis and flow direction (°)

γ activity coefficient

δ film thickness (m)

ε porosity of column

λ heat diffusivity (m^2/s)

μ dynamic viscosity (kg/ms)

ρ density (kg/m^3)

φ corrugation inclination angle (with respect to column axis) (°)

Subscripts

G referring to gas

in entrance flow

L referring to liquid

out exit flow

rxn reaction

Superscripts

aq aqueous

f formation

g referring to gas

ig ideal gas

is ideal solution

l referring to liquid

lv liquid to vapor

ref reference state

sat saturation

INTRODUCTION

Natural gas is considered sour if H_2S and CO_2 are present in more than standard amounts in the gas. In this case, before the gas can be utilized, H_2S and CO_2 must be removed and this is called gas sweetening. The gas is usually sweetened by absorption of the H_2S and CO_2 into an amine solution in a classical sieve plate column. Natural gas is one of the sources

of relatively clean energy and the demand for it is increasing rapidly. The effective purification of this energy source requires more sophisticated equipment since a huge amount of gas should be processed daily. The new generation of columns, called structured packed beds, which offer better mass transfer and relatively low pressure drop, are one such type of equipment [1-9]. Mathematical modeling of absorption of acid gas into MDEA (methyl diethanol amine) in structured packing requires a comprehensive model for liquid and gas flow in the bed. Localization of boundaries regarding the two phases, except for simple motions such as films, jets, etc. is practically impossible due to intricate interphase interactions dictated by packing geometry and surface characteristics. In addition, it is necessary to model the chemical absorption of acid gases into MDEA. There are mainly two approaches for modeling of gas absorption in the literature. The first assumes thermodynamic equilibrium for both streams leaving each stage and its idealization is compromised by introducing HETP (height equivalent to a theoretical plate) [10]. This parameter has to incorporate many other parameters affecting the operation of the column, including packing type, size and material. The so called rate-based approach, which appears more realistic, directly considers mass and heat transfer [11-13]. In most of these studies film or penetration theories are applied for prediction of the rate of mass transfer in liquid and gas. Two-film theory, which has gained more acceptance and understanding, considers that molecular diffusion occurs solely in two thin adjacent films near the interphases and there exists no concentration gradient outside this film to a high degree of mixing in the bulk [10]. The Accuracy of film theory model depends upon good estimation of film thickness. Also, multicomponent mixtures are characterized by several diffusion coefficients related to different component binary pairs, and therefore, the film thickness is different for each component.

In 1972, Zogg investigated the performance of structured packings equipped with Sulzer BX and Sulzer BY gauze packings [14]. A similar model for mass transfer in gauze packings was proposed by Bravo *et al*. [1] and then by Fair and Bravo [15], and Rocha *et al*. [1, 3, 4], to include the expected incomplete surface wetting for structured packings of the corrugated sheet type. They considered the gas flow in structured packings as passing through a series of wetted-wall columns with the dimensions related to the actual angle and size of the corrugations. Olujic [5, 7] proposed a model which represents the packings as a bundle of wetted wall channels with the characteristic triangular cross-section. In some other studies liquid motion is approximated by the film flow over an inclined surface [16, 17]. A fairly comprehensive literature survey about structured packings was done by Shilkin *et al*. [9].

In 2004, Ludovic Raynal worked on determination of mass transfer characteristics of co-current two-phase flow within structured packing. Both physical and chemical methods were used to determine the mass transfer performance of structured packing for gas-liquid absorption under co-current downward operation [18]. Absorption of nitrogen oxides in aqueous solutions in a structured packing pilot column was investigated by de Paivain in 2005. This study deals with the absorption of dilute nitrogen oxides NO_x into aqueous solutions of hydrogen peroxide and of sodium hydroxide at atmospheric pressure. A pilot column filled with the structured metallic packing Optiflow[TM] was employed [19]. Thin film flow over structured packings was also studied by Prashant Valluri in 2005. The model describes the dynamic evolution of waves on laminar falling wavy films at low to moderate Reynolds numbers over corrugated surfaces [20]. Recently, in 2007, a multi-scale approach was used by Raynal for CFD calculations of gas–liquid flow within a large-size column equipped with structured packing. This study focuses on the CFD modeling of the two-phase flow within a complex geometry. It first considers liquid–wall and liquid–gas interactions on a small scale via two-phase flow calculations using the (volume of fluid) VOF method. Second, the latter results are used in three-dimensional calculations run on a meso-scale corresponding to a periodic element representative of the real packing geometry. Last, those results are further used on a large scale in three-dimensional calculations with a geometry corresponding to a complete column [21].

As can be seen from the above discussion, there is still controversy in the selection of the best approach for modeling the absorption of acid gases into MDEA in the structured packed column. The first choice is to consider all the realistic phenomena in the process. For instance, one can consider turbulency in the gas and liquid, and also take different values for diffusivity of species in the liquid and consider that the entire surface is not wetted with the liquid. In this case it is very hard to localize the boundaries between liquid and gas and almost impossible to write equations of mass, momentum and energy balances. The second choice is to simplify the process, as is the case in the Shilkin model, in which the flow of liquid and gas is assumed to be laminar. It should be noticed that taking even these idealistic conditions usually results in good and valuable knowledge of the process and paves the way for reliable design on an industrial scale. In the present paper geometric calculations, phase boundary localizations and conditions used in the modeling of Shilkin *et al*. [9] are applied for mathematical modeling of chemical absorption of acid gases into MDEA in a structured packed bed. The geometric calculations regarding the packings as well as velocity equations for gas and liquid are similar to those utilized in Shilkin's work.

1 GEOMETRIC CHARACTERISTICS AND FLUID FLOW IN STRUCTURED PACKINGS

A complicated liquid flow over a packing surface which is made by corrugated sheets *(Fig. 1)* manufactured from
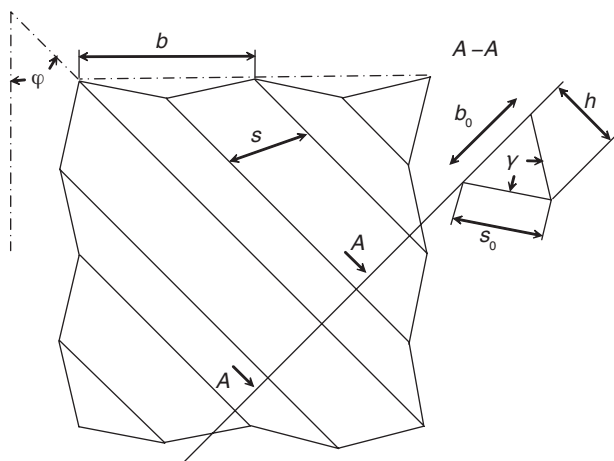
Figure 1

Geometry structure of a corrugated sheet, adopted from
Reference [9].

gauze, metal, ceramics or plastics is simplified to a laminar
film flow. This simplification lets us localize phase bound-
aries and specify boundary conditions. Therefore, continuum
mechanics equations of flow can be solved for the system.

Typical corrugated sheet structured packings are composed
of a number of segments perpendicular to each other to
produce the mixing effects for both gas and liquid at each
transition from one packing segment to another. The packing
segment can be visualized as a set of channels formed from
counter-course installation of corrugated sheets. The detail
of the shape of a segment of a typical corrugated sheet struc-
tured packing is given elsewhere [9].

Channels formed by corrugated sheets cross each other at
an angle of φ and are assumed to have identical cross-section
areas. Each channel is formed by the two wall sides s_0 and
one open side b_0, which faces a neighboring channel and is
shared between the two channels [17].

Based on previous studies [7, 9, 15], we assume that:
– the gas flow through a packing segment can be approxi-
  mated by a flow through a bundle of channels with dimen-
  sions derived from the corrugation geometry of Figure 1;
– channels are round;
– the gas and liquid flows in the channels are laminar and
  fully developed;
– under influence of gravity (as in this case), liquid gener-
  ally tends to move in the form of laminar films at the min-
  imal angle with the column axis, corresponding to the
  gravity flow angle α (see *Fig. 2*);
– gas and liquid are ideally mixed at certain points dictated
  by geometric configuration. These points, which are called
  mixing points, will be discussed in the following sections.
  For all channels, the film thickness is the same. This
  means that any radial maldistribution is neglected.

The inner diameter of a channel is set equal to the hydraulic
diameter of the corresponding triangular channel:

$$d_h = \frac{b_0 h}{s_0} \tag{1}$$

Mixing points are assumed in each channel for liquid and
gas where they are fully mixed because of abrupt changes in
gas and liquid flow. Shilkin assumed the length of the undis-
tributed laminar flow to be equal to an average channel
length in a packing segment. These mixing points are calcu-
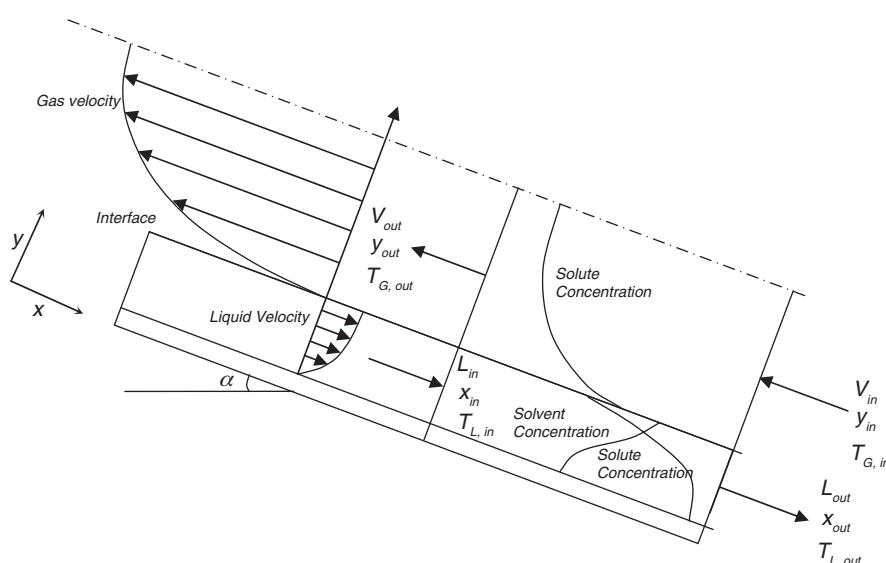lated separately for each phase [9].

Figure 2

Schematic of flow of liquid and gas, and concentration distribution in the channels.

M Baniadam et al. / *Comparison of Separation Performance of a Structured Packed Column with a Tray-Type Column for H$_2$S and CO$_2$*

183

$$z_L = \frac{b_0}{2\sin(\gamma/2)\sin(\arcsin(\sin\varphi\cos(\arctan(\cos\varphi\cot(\gamma/2)))))} \quad (2)$$

Total channel length is given by the following relation:

$$B_i = \sqrt{D_{pac}^2 - (h(n - 2(i-1)))^2} \quad (3)$$

$$l_i = \frac{2B_iL}{b_0}, \quad i = 1, \ldots, n \quad (4)$$

$$n = \left[\frac{D_{pac}}{h}\right], \quad k = \left\{\frac{1}{2}n\right\} \quad (5)$$

By [ ] we mean nearest smaller integer number and by { } we mean rounded off to the nearest bigger integer number.

The average channel length is given for even and odd n as follows:

$$z_G = \frac{2L\sum_{i=1}^{k}B_i}{2\cos\varphi\sum_{i=1}^{k}B_i + k(2L\sin\varphi - b_0)}, \quad n \text{ is even} \quad (6)$$

$$z_G = \frac{2L\left(2\sum_{i=1}^{k}B_i + B_k\right)}{2\cos\varphi\left(2\sum_{i=1}^{k}B_i + B_k\right) + (2k-1)(2L\sin\varphi - b_0)}, \quad (7)$$

$$n \text{ is odd}$$

The total inner surface of the channels comprising a packing segment is related to the packing geometric (installed) area S_t, whereas their wetted surface is related to the packing effective (wetted) mass transfer area S_e. However, both surfaces are assumed to be the same.

$$S_t = a_t \frac{\pi D_{pac}^2}{4} L \quad (8)$$

$$S_e = a_e \frac{\pi D_{pac}^2}{4} L \quad (9)$$

Hydraulic boundary conditions for liquid, gas and the interphase are considered as follows:

On the sheet wall (liquid):

$$y = 0, \quad u_L = 0 \quad (10)$$

On the interphase:

$$y = \delta, \quad u_L \frac{\partial u_L}{\partial y} = u_G \frac{\partial u_G}{\partial y} \quad (11)$$

On the channel symmetry axis:

$$y = R_h = \frac{d_h}{2}, \quad \frac{\partial u_G}{\partial y} = 0 \quad (12)$$

By application of the system of Navier–Stokes equations in the film flow approximation *(Fig. 2)* and using necessary boundary conditions, the following parabolic form for velocity distribution is found [9]:

$$u_p = A_p y^2 + B_p y + C_p, \quad p = L, G \quad (13)$$

The coefficients of Equation (13) can be found by applying boundary conditions and conservation of momentum and mass concepts in the following form:

$$A_L = \frac{\Delta P + \rho_L g \sin\alpha}{2\mu_L} \quad (14)$$

$$A_G = \frac{\Delta P + \rho_G g \sin\alpha}{2\mu_G} \quad (15)$$

$$B_G = -2A_G R_h \quad (16)$$

$$C_L = 0 \quad (17)$$

$$\mu_L(2A_L\delta + B_L) = \mu_L(2A_G\delta + B_G) \quad (18)$$

$$q_G = w_G\left(A_G \frac{R_h^3 - \delta^3}{3} + B_G \frac{R_h^2 - \delta^2}{3} + C_G(R_h - \delta)\right) \quad (19)$$

Also, the following expression for the determination of the liquid film thickness δ can be derived:

$$\frac{g w_G \delta (R_h - \delta)^2 (\rho_L - \rho_G)(3\mu_G\delta + 4\mu_L(R_h - \delta))\sin\alpha}{6\mu_G\mu_L(3R_h - \delta)}$$
$$+\frac{q_L w_G(\delta - R_h)(3\mu_G\delta(2R_h - \delta) + 2\mu_L(R_h - \delta)^2)}{\mu_G w_L \delta^2(3R_h - \delta)}$$
$$-q_G = 0 \quad (20)$$

2 HEAT AND MASS TRANSFER

The liquid consists of water (H$_2$O), MDEA, and dissolved CO$_2$ and H$_2$S, and ion species such as hydronium (H$_3$O$^+$), hydroxide (OH$^-$), bicarbonate (HCO$_3^-$), carbonate (CO$_3^{2-}$), bisulfide (HS$^-$), sulfide (S^{2-}) and protonated MDEA (R$_2$R'NH$^+$). These ions are produced from the following equilibrium reactions:
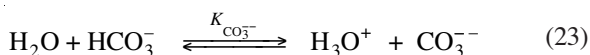
Water Dissociation:

$$2\,H_2O \xrightleftharpoons{K_{H_2O}} H_3O^+ + OH^- \quad (21)$$

Bicarbonate Formation:

$$2\,H_2O + CO_2 \xrightleftharpoons{K_{HCO_3^-}} H_3O^+ + HCO_3^- \qquad (22)$$

Carbonate Formation:

$$H_2O + HCO_3^- \xrightleftharpoons{K_{CO_3^{--}}} H_3O^+ + CO_3^{--} \qquad (23)$$

Bisulfide Formation:

$$H_2O + H_2S \xrightleftharpoons{K_{HS^-}} H_3O^+ + HS^- \qquad (24)$$

Sulfide Formation:

$$H_2O + HS^- \xrightleftharpoons{K_{S^{--}}} H_3O^+ + S^{--} \qquad (25)$$

MDEA protonation:

$$H_2O + R_2R'NH^+ \xrightleftharpoons{K_{MDEAH^+}} H_3O^+ + R_2R'N \qquad (26)$$

The reaction rate of amine with carbon dioxide is expressed as:

$$-r_{MDEA-CO_2} = k_I\, C_{B_2}\left(C_{A_1} - \frac{C_{E_2}}{K_{HCO_3^-}\, C_{OH^-}}\right) \qquad (27)$$

The reaction of CO_2 with water or bicarbonate formation is neglected due to the low rate constant and other reactions are assumed to be instantaneous. The equilibrium constants and rate of alkanolamine reactions with the acid gases H_2S and CO_2 are documented by Austgen (1989) and Glasscock (1990), respectively. The concentrations of H_2O, H_3O^+, CO_3^{2-} and S^{2-} in the liquid film are set equal to their respective liquid equilibrium concentrations and invariant across the liquid film. Based on the above discussion, it is possible to write six differential equations for the six species CO_2 (A_1), H_2S (A_2), MDEA (B_2), HCO_3^- (E_2), HS^- (E_3) and $MDEAH^+$ (F_2) in the liquid. The symbols in parenthesis are introduced to simplify the notations. The six differential equations are given by:

CO_2:

$$\frac{\partial^2 C_{A_1}}{\partial y^2} = -\frac{1}{D_{A_1}}\left(r_{B_2-A_1} + u_L(y)\frac{\partial C_{A_1}}{\partial x}\right) \qquad (28)$$

H_2S:

$$\frac{\partial^2 C_{A_2}}{\partial y^2} = \frac{1}{D_{A_2}}\left(r_{B_2-A_1} + u_L(y)\left(\frac{\partial C_{A_2}}{\partial x} - \frac{\partial C_{B_2}}{\partial x}\right) + D_{B_2}\frac{\partial^2 C_{B_2}}{\partial y^2}\right) \qquad (29)$$

MDEA:

$$\frac{\partial^2 C_{B_2}}{\partial y^2} = \frac{1}{C_{A_2}\, k_{A_2-B_2}}$$
$$\left(2\left(1+C_{E_3}\right)\frac{\partial^2 C_{E_3}}{\partial y^2} + C_{E_3}\frac{\partial^2 C_{E_2}}{\partial y^2} + C_{E_2}\frac{\partial^2 C_{E_3}}{\partial y^2} + 2\frac{\partial C_{E_2}}{\partial y}\frac{\partial C_{E_3}}{\partial y}\right) \qquad (30)$$
$$+ \frac{1}{C_{A_2}}\left(-2\frac{\partial C_{A_2}}{\partial y}\frac{\partial C_{B_2}}{\partial y} - C_{B_2}\frac{\partial^2 C_{A_2}}{\partial y^2}\right)$$

HCO_3^-:

$$\frac{\partial^2 C_{E_2}}{\partial y^2} = -\frac{1}{\bar{D}}\left(r_{B_2-A_1} + u_L(y)\frac{\partial C_{E_2}}{\partial x}\right) \qquad (31)$$

HS^-:

$$\frac{\partial^2 C_{A_2}}{\partial y^2} = \frac{1}{\bar{D}}\left(-r_{B_2-A_1} + u_L(y)\left(\frac{\partial C_{E_3}}{\partial x} + \frac{\partial C_{B_2}}{\partial x}\right) - D_{B_2}\frac{\partial^2 C_{B_2}}{\partial y^2}\right) \qquad (32)$$

$MDEAH^+$:

$$\frac{\partial^2 C_{F_2}}{\partial y^2} = \frac{1}{\bar{D}}\left(u_L(y)\left(\frac{\partial C_{F_2}}{\partial x} + \frac{\partial C_{B_2}}{\partial x}\right) - D_{B_2}\frac{\partial^2 C_{B_2}}{\partial y^2}\right) \qquad (33)$$

It should be noticed that no reaction is considered in the gas, and thus governing partial differential equations of mass transfer for nonreacting species in liquid and all presented components in the gas are given in the following equations:

$$\frac{\partial^2 C_{i,L}}{\partial y^2} = \frac{1}{D_{i,L}}\, u_L(y)\frac{\partial C_{i,L}}{\partial x} \qquad (34)$$

$$\frac{\partial^2 C_{i,G}}{\partial y^2} = \frac{1}{D_{i,G}}\, u_G(y)\frac{\partial C_{i,G}}{\partial x} \qquad (35)$$

The concentration of the hydroxide ion may be related to the concentrations of MDEA, $MDEAH^+$ and H_2O by the equilibrium relation:

$$C_{OH^-} = \frac{K_{H_2O}\, C_{MDEA}\, C_{H_2O}}{K_{MDEAH^+}\, C_{MDEAH^+}} \qquad (36)$$

In the inlet of each segment, bulk concentrations of H_2O, H_3O^+, CO_3^{2-} and S^{2-} are calculated by the method of Barreau *et al.* [22]. Concentrations of these components are either too low, such as H_3O^+, CO_3^{2-} and S^{2-}, or too high, such as H_2O, which are reasonably assumed to be invariant until we reach the next segment.

M Baniadam et al. / *Comparison of Separation Performance of a Structured Packed Column with a Tray-Type Column for H$_2$S and CO$_2$*

185

The diffusivity of CO_2 in the reactive solution was approximated by the N_2O analogy proposed by Versteeg and van Swaaij [23], the diffusivity of H_2O in the solution was approximated by $1.02\, D_{CO_2}$ using the Wilke-Chang formula [24], and the alkanolamine diffusivity was approximated using the modified Stokes-Einstein equation as proposed by Glasscock [25].

The ion diffusion coefficient D_i is assumed to be invariant in the liquid film. Regardless of the size, the charged species diffuse at a rate that maintains the solution electrically neutral. Thus, D_i, for any charged species, depends on the concentrations of all charged species present. In this study, to preserve electro-neutrality the diffusion coefficients of all ions are set equal so Equations (31-33) can be used. The diffusivities of all ions are set equal to a molar average diffusion coefficient, $\overline{D}$:

$$\overline{D}_i = \frac{\sum\limits_{i} x_i}{\sum\limits_{i} \dfrac{x_i}{D_i}} \tag{37}$$

where $\overline{D}_i$ and x_i are the intrinsic diffusivity and the mole fraction of ion i, respectively. The heat transfer equations for gas and liquid are:

$$k_L \frac{\partial^2 T}{\partial y^2} = \frac{\partial}{\partial x}\left(u_L(y)\frac{\rho}{\overline{M}}\sum x_i \overline{h}_i^{liq} \right), \tag{38}$$

$$\alpha_G \frac{\partial^2 T}{\partial y^2} = u_G(y)\frac{\partial T_G}{\partial x}$$

where $\overline{h}_i^{liq}$ is the partial molar enthalpy of component i in liquid. This term can be expressed in terms of an ideal solution molar enthalpy, h_i^{is}, and an excess molar enthalpy, h_i^{ex}, according to:

$$\overline{h}_i^{liq}(T,P,x) = h_i^{is}(T,P) + h_i^{ex}(T,P,x) \tag{39}$$

Neglecting the effect of pressure, the ideal solution molar enthalpy for solvents such as water and alkanolamine is given by:

$$h_i^{is}(T,P) \approx h_i^{is}\left(T,P_{H_2O}^{sat}\right) = \Delta h_i^{f,ig}\left(T^{ref}\right)$$
$$+ \int_{T^{ref}}^{T} C_{P,i}^{ig}(T)\,dT - RT^2 \frac{\partial \ln\left(h_{i,H_2O}\right)}{\partial T} \tag{40}$$

where $\Delta h_i^{lv}(T)$ is the heat of vaporization of solvent evaluated at the system temperature.

For molecular solutes such as CO_2 and H_2S, the corresponding ideal solution molar enthalpy is given by:

$$h_i^{is}(T,P) \approx h_i^{is}\left(T,P_{H_2O}^{sat}\right) = \Delta h_i^{f,ig}\left(T^{ref}\right)$$
$$+ \int_{T^{ref}}^{T} C_{P,i}^{ig}(T)\,dT - RT^2 \frac{\partial \ln\left(h_{i,H_2O}\right)}{\partial T} \tag{41}$$

The ideal solution molar enthalpy for ionic species is given by:

$$h_i^{is}(T,P) \approx \Delta h_i^{f,aq}(298.15) + C_{P,i}(T - 298.15) \tag{42}$$

where $\Delta h_i^{f,aq}$ is the heat of formation of an ion, i, at infinite dilution in water. The excess Gibbs free energy measures the deviation of the system from ideality. All other thermodynamic excess properties can be derived from the excess Gibbs free energy relations. Since this property is related to the species activity coefficients the excess molar enthalpies of species i, h_i^{ex}, have a similar relationship. This relationship is given by:

$$h_i^{ex} = -RT^2 \left(\frac{\partial \ln \gamma_i}{\partial T} \right)_x \tag{43}$$

In Equation (43) it is assumed that pressure has a negligible effect on the excess molar enthalpy. The activity coefficients of all species are computed from the electrolyte-NRTL model at specified system temperature, acid gas loadings and alkanolamine initial percent. The excess molar enthalpies of all species are determined by numerically differentiating the activity coefficient of each species with respect to temperature at fixed species mole fractions.

Boundary conditions are formulated as follows [9]:

At the entrance of liquid:

$$x = 0, \qquad C_L = C_L^{in}, \qquad T_L = T_L^{in} \tag{44}$$

At the entrance of gas:

$$x = L, \qquad C_G = C_G^{in}, \qquad T_G = T_G^{in} \tag{45}$$

At the wall (adiabatic and non-permeable):

$$y = 0, \qquad \frac{\partial C_L}{\partial y} = 0, \qquad \frac{\partial T_L}{\partial y} = 0 \tag{46}$$

At the channel symmetry axis:

$$y = R_h, \qquad \frac{\partial C_G}{\partial y} = 0, \qquad \frac{\partial T_G}{\partial y} = 0 \tag{47}$$

At the phase interface (thermodynamic equilibrium, mass and energy conservation conditions):

$$y = \delta, \quad C_G = [K_i]C_L \quad T_L = T_G,$$

$$[D_L]\frac{\partial C_L}{\partial y} = [D_G]\frac{\partial C_G}{\partial y} + r_L\Big|_{y=\delta} \tag{48}$$

$$\lambda_L \frac{\partial T_L}{\partial y} = \lambda_L \frac{\partial T_L}{\partial y} + (\Delta H_{rxn})^T [D_L]\frac{\partial C_L}{\partial y}$$

$r_L\big|_{y=\delta}$ is the rate of surface reaction and is zero for all components other than H_2S, which has an instantaneous reaction with amine.

The surface reaction terms appearing in Equation (48) are obtained from stoicheiometry as follows:

$$r_{A_2}\Big|_{z=0} = r_{B_2}\Big|_{z=0} = D_{B_2}\frac{d\,C_{B_2}}{d\,z}\Big|_{z=0} \tag{49}$$

Film concentration distribution is not known at first and is calculated in a trial-and-error procedure.

Reynolds numbers for gas and liquid streams are calculated in the following form:

$$\text{Re}_G = \frac{\dot{m}_G\,L\,d_h}{S_t \sin\alpha\,(R_h - \delta)\mu_G} \tag{50}$$

$$\text{Re}_L = \frac{\dot{m}_L\,L\,d_h}{S_e \sin\alpha\,\delta\mu_L} \tag{51}$$

3 METHOD OF SOLUTION

For the known parameters of the column (D_p, γ, φ, etc.) an arbitrary height was assigned for the column. With known inlet conditions, the following sequential steps were taken to solve Equations (28) through (48) for the assigned value of the height:

– All geometric dimensions of the column were calculated by using Equations (1) through (9).
– Having inlet gas and liquid information and guessing the exiting gas stream, overall material and energy balances for the column will provide the exiting liquid stream. After this, the column height starting from the bottom was divided into segments of 0.183 meters. The following calculations were carried out for all the segments starting with the first segment for which (at the bottom of the column) the conditions of entering gas and exiting liquid are known.
– The space of the segment was discretized in and directions and mass balance Equations (28) through (35), which included velocity distribution, Equations (13-20), and energy balance, Equation (38), with their boundary conditions of (44) through (48) were applied in each point of discretized space.

– The rate of reaction at the surface for H_2S in Equation (48) was set equal to zero for the first iteration.
– The nonlinear algebraic equations resulting from discretization in step 3 were solved by Newton's global convergence method. The advantage of this method is that it is not too sensible to the initial guess. The results of these equations give temperature and concentration distribution over the segment. Instead of setting the rate of reaction equal to zero for H_2S at the surface, after the first iteration the following two steps were taken to calculate it.
– Concentration distribution calculated in step 5 gives the new value for the rate of surface reaction using Equation (49). This rate is compared with what is guessed in step 4 and its iterations are repeated until the difference between new and old values of the rate varies within a specified range.
– Temperature and concentration of exiting streams from one segment are the inlet information for the next segment. A uniform distribution is assumed in the direction for each segment.
– This procedure is repeated from the bottom to the top of the column. When the calculation is carried out for the last segment (top of the column) the conditions of the exiting gas stream will be calculated. This information was also guessed in step 2. Comparing calculated and guessed information about the exiting gas stream indicates whether repeating iteration is necessary or not for that assigned height.
– The assigned value of the height of the column was changed and all the steps were carried out. The change in value of height and carrying out the calculations were repeated until a reasonable agreement was noticed between estimated and calculated information for the exiting gas stream in the tray column.

4 RESULTS AND DISCUSSIONS

Montz-Pak A3-500 packings are used for solution of the mathematical modeling of acid gas absorption. The geometric specifications of structured packing and model parameters are listed in Table 1.

TABLE 1

Geometric characteristics and model parameters of the bed, Montz-Pak A3-500 packings

a_t (m²/m³)	500	d_h (m)	0.0045
ε (–)	0.95	R_h	0.00225
h (m)	0.006		66.5
b_0 (m)	0.009	z_L (m)	0.0228
s_0 (m)	0.0075	z_G (m)	0.2024
L (m)	0.183	S_t (m²)	602.293
γ (°)	74	S_e (m²)	602.293
φ (°)	30	D_p (m)	2.895

M Baniadam et al. / *Comparison of Separation Performance of a Structured Packed Column
with a Tray-Type Column for H₂S and CO₂*

187

TABLE 2

Specifications of column with sieve trays

Diameter (m)	Height (m)	No. of trays	Bubble area (cm²)	Active area (cm²)	Diameter of holes (cm)	Weir height (cm)	Tray spacing (cm)
2.895	16.46	20	3393.5	42411.96	0.5556	14.1	80

TABLE 3

Conditions of feed gas (sour), lean amine, sweet gas and rich amine streams

	% H_2S	% CO_2	% CH_4	% H_2O	% MDEA	F (kmol/h)	T (K)	Pressure (kPa)
Sour gas	3.85	6.41	89.71	0.03	–	635.40	294.1	7401
Lean amine	–	–	–	91.89	8.11	1606.8	350	7506
Sweet gas	4ppm	2.55	97.16	0.29	–	565.55	329.4	7506
Rich amine	1.46	1.57	1.22	87.98	7.77	1676.65	327.1	7401

Since there was no plant data for the absorption of acid gases by MDEA solution in a structured column with corrugated sheets on an industrial scale, therefore it was not possible to validate the model by plant data. We were forced to compare the performance of operating a sieve tray column (see *Table 2*) with a structured packed column. Different heights for the column were assigned, and according to the results of mathematical modeling of the structured packed column, it was found that at the height of 8.14, the degree of purification for acid gases in the structured packed bed and the operating sieve tray column is the same.

The performance of the modeled tray column was validated previously against operational data of an industrial sweetening absorption column.

A set of data for a CO_2-H_2S-MDEA absorber that is utilized in the solution of the model is shown in Table 3. The operating parameters are adjusted so that the flow of liquid and gas in the column are laminar.

Two Visual Basic programs were written to solve the governing equations of the model (1-9, 13-20 and 28-49). The task of the first program is to solve Equations (1-9) and Equations (13-20) and find the velocity distribution of gas and liquid in each part of the column. Having the velocity distribution in liquid and gas, the second program is used to solve governing equations relating to the mass and heat transfers (28-49). Both mentioned programs are implemented in a main program, so the second program takes advantage of the results of the first program for calculation of temperature and concentration distribution.

Figure 3 shows the velocity distribution resulting from the solution of hydrodynamic equations. Although the composition of the liquid differs from its correspondent value in Shilkin's paper due to the nature of the solvent and solute, the velocity distribution of liquid is in good agreement with results reported by Shilkin *et al*. Reynolds numbers for both liquid and gas streams are calculated according to Equations (50) and (51) at different parts of the structural column. The calculated Reynolds numbers are in the range of 100-200,
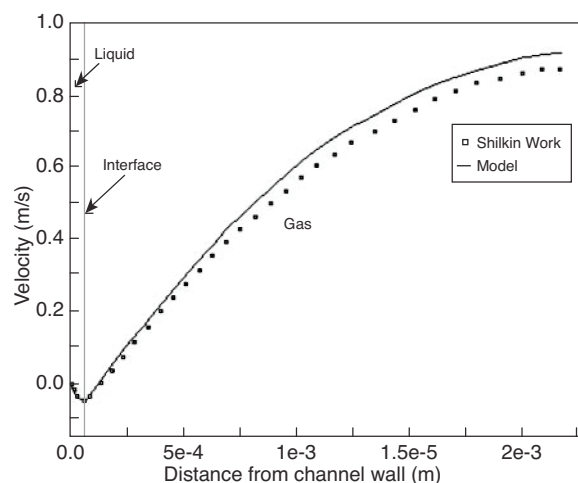

Figure 3

Calculated velocity F_L = 635.40 kmol/h, T_L = 294.1 K.

which are far from 2100, and therefore it can be fairly assumed that a laminar region prevails in gas and liquid streams.

Figure 4 shows that the composition profile of H_2S in the system exhibits three different regions depending on the location in the absorber. At the bottom of the absorber, region I, there is a little tendency for H_2S to get absorbed, as appears from the relatively moderate decrease in the mole fraction. At the middle stages, region II, there is a dramatic increase in the H_2S absorption rate, causing its mole fraction to approach the specified value. At the top of the absorber region III, it becomes extremely difficult to absorb H_2S, although there is an appreciable driving force, as indicated from the difference between the equilibrium and actual compositions of H_2S. The H_2S composition profiles show that the MDEA system has
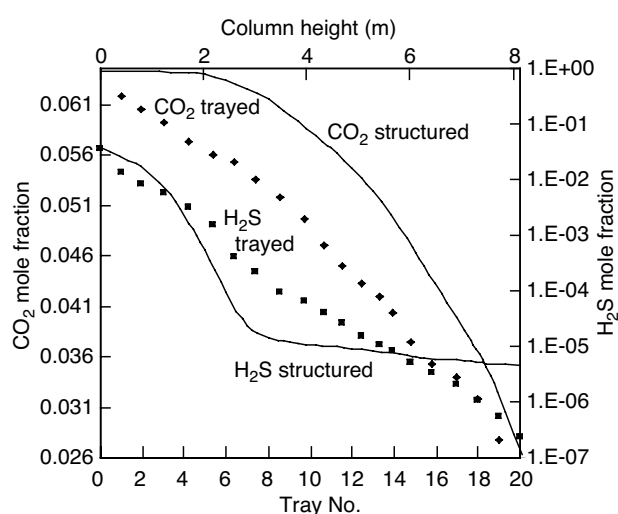
Figure 4

H_2S and CO_2 mole fractions in gas *versus* height for a system of CO_2-H_2S-MDEA in structured packing and tray columns.
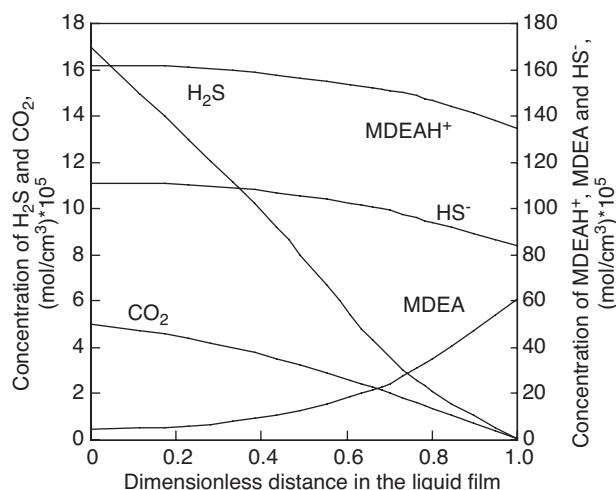

Figure 5

Typical concentration profiles in the liquid film *versus* dimensionless distance (y/δ) from the wall for distance = 3 m from the top of the column.

column is more difficult because no change in the mole fraction of H_2S is seen. Therefore, we can conclude that in a structured column we could achieve more H_2S purification by increasing the height of the column.

The composition profile of CO_2 is also shown in Figure 4. As seen from this figure, the composition of CO_2 is virtually constant at the bottom of the absorber, region I. The high concentration of the acid gases in addition to the scarcity of the amine in this region makes the competition between CO_2 and H_2S to react with the amines extremely difficult. Due to the instantaneous reaction that occurs between H_2S and the amines, H_2S consumes most of the amines present, leaving a negligible amount to react with CO_2. The competition continues to region II where the driving forces of both gases and the amine concentrations are higher. In this region the capacity of the amines is just enough to contain both gases. However, H_2S, which has a faster tendency to react with the amines, continues to consume most of the amines until its absorption driving force diminishes. In region III, the CO_2 driving force becomes too large, reducing further consumption of the amines by H_2S. This makes extra purification of H_2S extremely difficult to achieve. As observed from this figure, the absorption driving force of both gases is minimized at the bottom of the absorber. In the middle of the tower, which corresponds to region II, the driving force of H_2S becomes higher. It then diminishes to a steady value all the way to the top of the absorber. For CO_2, the driving force continues its increasing trend to the top of the absorber. Due to the extremely slow reaction of CO_2 with MDEA, the absorption of CO_2 does not start until H_2S reaches equilibrium. This explains why this system is the fastest to meet the specification of H_2S. The trend of absorption of CO_2 in the tray tower is similar to the structured column; however, the rate
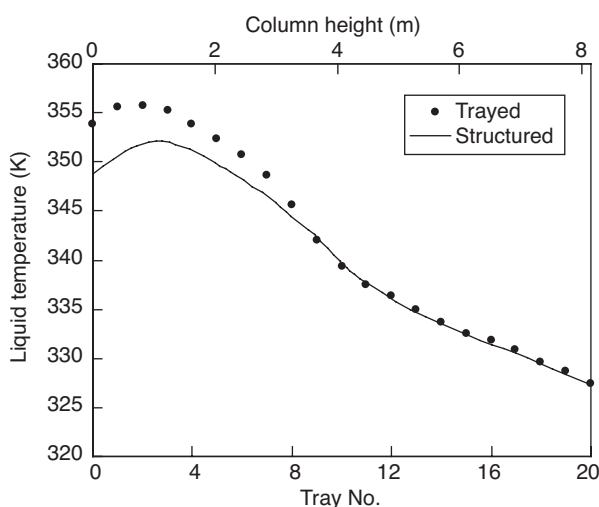

Figure 6

Liquid temperature *versus* height for CO_2-H_2S-amine towers.

the best performance in regions II and I. However, in region III, the ability of MDEA to absorb H_2S becomes so poor that the composition of H_2S remains virtually unchanged. This is attributed to the presence of CO_2, which strongly competes with H_2S in the consumption of amines, specially at the top of the absorber where the concentration of CO_2 is much higher than H_2S. Overall behavior in absorption of H_2S for both tray and structured columns are nearly the same. However, as Figure 4 shows, absorption of H_2S in the tray

M Baniadam et al. / *Comparison of Separation Performance of a Structured Packed Column with a Tray-Type Column for H₂S and CO₂*

189

of absorption of CO_2 becomes relatively linear from tray no. eight.

The liquid film concentration profiles of the reacting species in the CO_2-H_2S-MDEA system at distance = 3 m from the top of the column is shown in Figure 5. In this figure the distance is measured dimensionlessly as in which is the thickness of the liquid flowing film. These profiles confirm the boundary conditions of solute species, as is expected. The slope of the profile of H_2S is greater than CO_2 and it can be related to instantaneous reaction between hydrogen sulfide and amine.

The temperature profile of the liquid is shown in Figure 6. The temperature profile of the CO_2-H_2S-MDEA system exhibits an inflated shape at the bottom of the absorber. The liquid temperature approaches the inlet gas temperature as we approach the top of the absorber. This system is fast to reach the inlet liquid temperature. This is attributed to the relatively negligible absorption of the acid gases by MDEA at the top of the absorber.

CONCLUSION

Absorption of the acid gases, H_2S and CO_2, by methyl diethanol amine in a structured column was modeled. In the mathematical model, channels are assumed to be an identical cross-section in which the walls are wetted completely by liquid and the rest of the channels are occupied with the acid gases. A film theory as well as a non-equilibrium rate-based concept were applied to modeling the mass and heat transfer phenomena in both directions of flow of liquid and gas. With the mathematical model we were able to investigate concentration and temperature profiles along the bed. The temperature profile of the CO_2-H_2S-MDEA system exhibits a temporary growth at the bottom of the absorber. The driving forces for absorption of both gases are at their lowest values at the top of the absorber and some sections of the column practically do nothing. This behavior is stronger in the tray column than the structure column. Therefore, one might conclude that under the same conditions, the structured packed bed column in general has better performance. The fact is that due to the lack of experimental data for the structured column of commercial size we had to validate the model of this column against the model of a tray-type column which was validated by plant data. This lack of plant or experimental data could cast a shadow over our last conclusion. However, with this study we have taken the first step toward modeling a very complicated physical situation.

ACKNOWLEDGMENT

REFERENCES

1 Bravo J.L., Rocha J.A., Fair J.R. (1985) Mass transfer in gauze packing, *Hydrocarb. Process.* 91-95.

2 Nawrocki P.A., Xu Z.P., Chuang K.T. (1991) Mass transfer in structured packing, *Can. J. Chem. Eng.* **69**, 1336-1343.

3 Rocha J.A., Bravo J.L., Fair J.R. (1993) Distillation columns containing structured packings: a comprehensive model for their performance. 1. Hydraulic models, *Ind. Eng. Chem. Res.* **32**, 641-651.

4 Rocha J.A., Bravo J.L., Fair J.R. (1996) Distillation columns containing structured packings: a comprehensive model for their performance. 2. Mass-transfer model, *Ind. Eng. Chem. Res.* **35**, 1660-1667.

5 Olujic Z. (1997) Development of a complete simulation model for predicting the hydraulic and separation performance of distillation columns equipped with structured packings, *Chem. Biochem. Eng. Q.* **11**, 1, 31-46.

6 Brunazzi E., Paglianti A. (1997) Liquid-film mass transfer coefficient in a column equipped with structured packing, *Ind. Eng. Chem. Res.* **36**, 3792-3799.

7 Olujic Z. (1999) Effect of column diameter on pressure drop of a corrugated sheet structured packing, *Chem. Eng. Res. Des.* **77**, 6, 505-510.

8 Billet R., Schultes M. (1999) Prediction of mass transfer columns with dumped and arranged packings: updated summary of the calculation method of Billet and Schultes, *Trans. IChemE* **77**, 498-504.

9 Shilkin A., Kenig E.Y. (2005) A new approach to fluid separation modeling in the columns equipped with structured packings, *Chem. Eng. J.* **110**, 87-100.

10 Taylor R., Krishna R. (1993) *Multicomponent Mass Transfer*, Wiley.

11 Al-Baghli N.A., Pruess S.A., Yesavage V.F., Selim M.S. (2001) A rate-based model for the design of gas absorbers for the removal of CO_2 and H_2S using aqueous solutions of MEA and DEA, *Fluid Phase Equilibr.* **185**, 31-43.

12 Taylor R., Kooijman H.A., Hung J.S. (1994) A second generation nonequilibrium model for computer simulation of multicomponent separation processes, *Comput. Chem. Eng.* **18**, 205-217.

13 Higler A.P., Taylor R., Krishna R. (1998) Modeling of a reactive separation process using a non-equilibrium stage model, *Comput. Chem. Eng.* **22**, S111-S118.

14 Zogg M. (1972) Stromungs- und Stoffaustauschunter-suchungen an der Sulzer-Gewebepackung, *Ph.D. thesis*, Technische Hochschule Zurich.

15 Fair J.R., Bravo J.L. (1990) Distillation columns containing structured packings, *Chem. Eng. Prog.* 19-29.

16 Johnstone H.F., Pigford R.L. (1942) Distillation in a wetted-wall column, *T. Am. Ind. Chem. Eng.* **38**, 25-50.

17 Kenig E.Y. (1997) Multicomponent multiphase film-like systems: a modeling approach, *Comput. Chem. Eng.* **21**, S355-S360.

18 Raynal L., Ballaguet J.P., Barrere-Tricca C. (2004) Determination of mass transfer characteristics of co-current two-phase flow within structured packing, *Chem. Eng. Sci.* **59**, 5395-5402.

19 de Paiva J.L., Kachan G.C. (2004) Absorption of nitrogen oxides in aqueous solutions in a structured packing pilot column, *Chem. Eng. Process.* **43**, 941-948.

20 Valluri P., Matar O.K., Hewitt G.F., Mendes M.A. (2005) Thin flow over structured packings at moderate Reynolds numbers, *Chem. Eng. Sci.* **60**, 1965-1975.

21 Raynal L., Royon-Lebeaud A. (2007) A multi-scale approach for CFD calculations of gas–liquid within large size column equipped with structured packing, *Chem. Eng. Sci.* **62**, 7196-7204.

22 Barreau A., Blanchon le Bouhelec1 E., Habchi Tounsi K.N., Mougin P., Lecomte F., (2006) Absorption of H_2S and CO_2 in Alkanolamine Aqueous Solution: Experimental Data and Modeling with the Electrolyte-NRTL Model, *Oil Gas Sci. Technol. – Rev. IFP* **61**, 3, 345-361.

23 Versteeg G., van Swaaij W. (1988) Solubility and Diffusivity of Acid Gases (CO_2, N_2O) in Aqueous Alkanolamine Solutions, *J. Chem. Eng. Data* **33**, 29-34.

24 Wilke C.R., Chang, P. (1955) *AIChE J.* **1**, 264-270.

25 Glasscock D.A. (1990) Modeling and Experimental Study of Carbon Dioxide Absorption into Aqueous Alkanolamines, Ph.D. Dissertation, The University of Texas at Austin, Austin, TX.